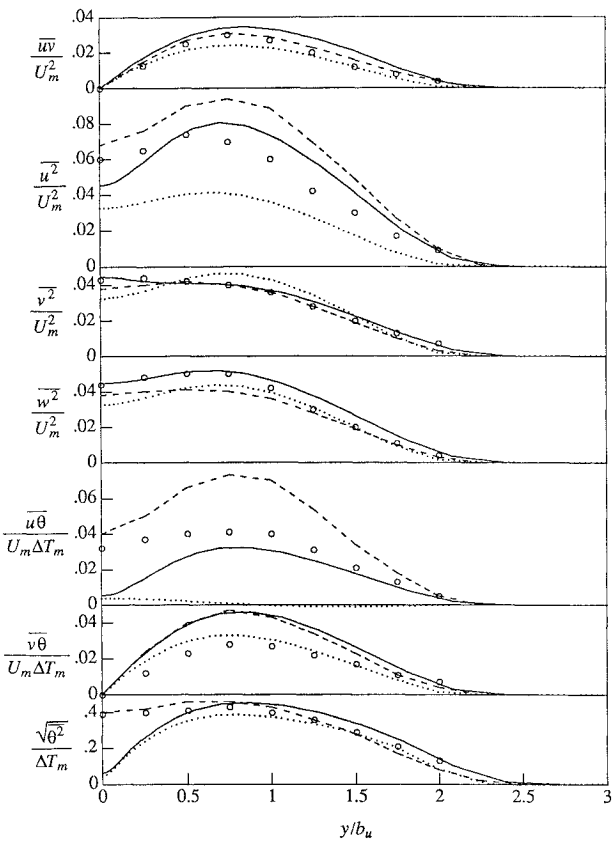

Fig. 1 Similarity profiles of Reynolds stresses, heat fluxes, and temperature fluctuations for a heated jet: — NAEV model, · · · SEV model, - - RS model,[5] o experiment.[4]

show a significant improvement over those obtained by the SEV model but are lower than the experimental data of Ramaprian and Chandrasekhara,[4] whereas the RS model[5] yields much higher results than the experimental data. In the case of the cross stream turbulent heat flux $\overline{v\theta}$ and temperature fluctuations $\overline{\theta^2}$, the three models predict different results, but the results predicted by the NAEV model are closer to those predicted by the RS model,[5] whereas the results of $\overline{v\theta}$ predicted by the SEV model display the closest agreement with the experimental data of Ramaprian and Chandrasekhara.[4]

B. Flow Past a Backward-Facing Step

This flow has served as a primary benchmark for the performance of turbulence models in the prediction of separated flows (e.g., Ref. 6). It is well known that the SEV model substantially underpredicts the reattachment point for this flow. The separation length (L/H, where H is the step height) is predicted by means of the SEV model as 5.7, whereas experiments indicate that it should be about 7.0.

The NAEV model predicts $L/H = 7.0$, which is a significant improvement over the result predicted by means of the SEV model. In comparison, the local equilibrium anisotropic model (i.e., in the NAEV model obtained with $f_\mu = 1$) predicts $L/H = 6.0$, whereas the nonequilibrium isotropic model (i.e., in the NAEV model obtained with $\alpha_1 = \alpha_2 = 0$) predicts $L/H = 7.0$. Thus, we can conclude that, for this flow, the improvement in the predictions of the separation length is essentially due to the fact that the NAEV model accounts for the nonequilibrium effects; the anisotropy of the flow has only a second-order effect.

Concluding Remarks

The NAEV model can effectively account for the nonequilibrium and anisotropic properties of a turbulent shear flow. This model is as equally capable as the RS model of accounting for buoyancy forces when the flow is heated, and it has the same advantages of numerical efficiency and stability as does the SEV model.

Acknowledgment

This research was sponsored by the National Research Council of Canada under Grant A-2746.

References

[1]Huang, P. G., and Leschziner, M. A., "Stabilization of Recirculating-Flow Computations Performed with Second-Moment Closures and Third-Order Discretization," *Proceedings of the Fifth Symposium on Turbulent Shear Flows* (Cornell, NY), 1985, pp. 20.7–20.12.

[2]Ni, W., "Numerical Prediction of the Statistical Properties of Heated Turbulent Air Jets in a Cross-Flow," Ph.D. Thesis, Univ. of Toronto, Canada, 1994.

[3]Rodi, W., *Turbulence Models and Their Application in Hydraulics*, International Association for Hydraulic Research, Delft, The Netherlands, 1980.

[4]Ramaprian, B. R., and Chandrasekhara, M. S., "Study of Vertical Plane Turbulent Jets and Plumes," IIHR 257, Univ. of Iowa, 1983.

[5]Malin, M. R., and Younis, B. A., "Calculation of Turbulent Buoyant Plumes with a Reynolds Stress and Heat Flux Transport Closure," *Journal of Heat and Mass Transfer*, Vol. 33, No. 10, 1990, pp. 2247–2264.

[6]Kim, J., Kline, S. J., and Johnston, J. P., "Investigation of a Reattaching Turbulent Shear Layer: Flow Over a Backward-Facing Step," *Journal of Fluids Engineering*, Vol. 102, Sept. 1980, pp. 302–308.

Shock Wave/Vortex Interaction in a Flow over 90-deg Sharp Corner

Naoki Uchiyama* and Osamu Inoue†
Tohoku University, Sendai 980-77, Japan

Introduction

A SHOCK wave diffraction over a 90-deg sharp convex corner provides one of the most basic flows in the field of compressible fluid dynamics. A variety of diffraction patterns dependent on incident shock Mach number has been extensively studied theoretically, experimentally, and numerically. However, it seems that the evolution process of a vortical flowfield near the corner has not been fully addressed compared to the shock wave diffraction process itself. For example, it is controversial whether or not secondary shock waves appearing in the vortical flowfield have a branch-like structure. Uchiyama and Inoue[1] suggest by computation that the branch-like structure may appear, although in experiments this structure has not been observed so far. This discrepancy may stem from some practical limitations in both experimental and computational studies. In the case of experiment, the characteristic time scale required for detectable growth of shear layer instability is relatively much larger than that for shock wave propagation and, hence, in order to capture distinct phenomena caused by shear layer instability, a pretty wide area of a test section is necessary. In the case of computation, capturing details of the flowfield such as rollup of the shear layer is not an easy task even with recent high-resolution schemes with large numbers of computational cells, since a numerical diffusion mechanism is inherent in any shock capturing scheme. To minimize the effect of numerical diffusion and to capture the vortex motion as accurately as possible under limited computer power, the use of adaptive mesh methods is desirable. In the present study, two-dimensional unsteady Euler computation with adaptive mesh refinement (AMR) algorithm[2] was performed to study the evolution process of a vortical flowfield generated near the corner. The results show that due to the growth of the Kelvin–Helmholtz instability, a

Received Sept. 6, 1994; revision received Feb. 17, 1995; accepted for publication Feb. 26, 1995.

*Graduate Student, Department of Mechanical Engineering, Institute of Fluid Science.

†Professor, Institute of Fluid Science. Member AIAA.

shear layer emanated from the corner rolls up to form discrete vortices. Successive interactions between the rolled-up vortices and the secondary shock waves, appearing in the vortical flow near the corner for a sufficiently large incident shock Mach number, are found to be responsible for the unsteady bifurcated branch-like structure of the secondary shock wave.

Flow Model and Numerical Methods

A schematic of the flow model is presented in Fig. 1. An incident shock wave propagates from left to right and diffracts at the 90-deg sharp corner of the wall. Behind the diffracted shock wave, a shear layer emanates from the corner and develops with increasing time. The two-dimensional Euler equations are numerically solved by a finite volume method formulated in Cartesian coordinates. The computational domain was prescribed to be a square with its side length $1.98L$, where L is a reference length that is set to unity.[3] As already mentioned, an AMR algorithm was adopted in the code to efficiently obtain the highly resolved flowfield, especially in the region of interest. The mesh system of the AMR algorithm consists of hierarchical multilevel submesh panels categorized by their mesh width. The coarsest mesh exists as an underlying base, whereas the submesh panels with finer mesh width are locally generated according to given criteria in order to dynamically adapt the local region of the flowfield. In this computation, we have allowed, at most, 3 levels of refinement. In Fig. 1, as an example, the locations of the adapted panels of the second and third levels are depicted by large and small square frames, respectively. The refinement ratio of the cell width between the neighboring levels were set to 5, with the coarsest mesh consisting of 99 cells in each direction. Thus, the finest mesh width on the third-mesh level is equivalent to the width of a cell in the case when the entire computational domain is uniformly divided by $99 \times 5 \times 5\,(=2475)$ cells in each directions. An explicit time integration is performed in a nested way so that after the solutions of the coarse base mesh are integrated one coarse time step, the solutions of the submesh panels are integrated successively with smaller time steps to catch up with the same time level.

Since our objective is to capture details of the vortical flowfield near the corner and the secondary shock waves in it, we have adopted for the mesh refinement indicator the blended value of the first and second local derivatives of the density which characterize shock waves and the magnitude of the vorticity which characterizes vortical flows. Further details on the algorithm are noted in Ref. 4. For the boundary conditions, a slip condition was applied to the walls of the corner block as well as to the top and bottom boundary of the computational domain. An outflow condition was applied at the right boundary of the computational domain, whereas the postshock condition was fixed at the left boundary of the computational domain. For the numerical flux evaluation, a flux vector splitting upwind scheme[5] was used with MUSCL extrapolation[6] in order to achieve higher order accuracy. To achieve second-order accuracy in time as well as space, a slight modification was made to the MUSCL approach by considering the time gradient of the conserved variables. In this computation, the medium considered is an ideal gas with specific heat ratio of $\gamma = 1.4$. The incident shock wave is initially set some distance upstream from the corner by numerically satisfying the Rankine–Hugoniot relations. The physical values were nondimensionalized by the ambient density ρ_∞ and the ambient speed of sound a_∞.

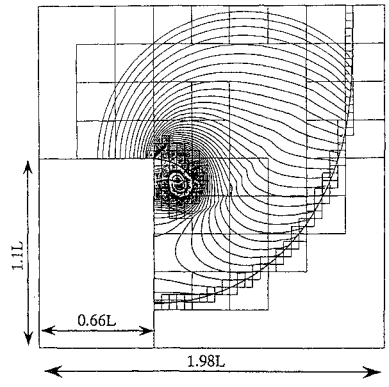

Fig. 1 Schematic of the overall flowfield.

Results and Discussion

We examined the flowfields for three different cases of the shock Mach number M_S of an incident shock wave: $M_S = 1.3$, 1.5, and 1.7. A typical example of a flowfield near the corner is shown in Fig. 2 for the case of $M_S = 1.5$ and $\bar{t} = 0.64$, where $\bar{t}$ is the nondimensional time scaled by L/a_∞. We can readily see a large-scale, vortical structure of the flowfield which was produced by the shear layer (SL) emanated from the corner. Hereafter this vortical structure is referred to as the corner vortex. In the figure, the Prandtl–Meyer expansion fan (EF) at the corner is terminated by a series of weak shock waves (SW1, SW2) along the shear layer to match the expanded flow with the condition behind the diffracted shock wave. A contact surface (CS) emanated from a point on the diffracted shock wave is observed under the corner vortex. Among these features, we are especially interested in the two distinct shock waves observed in the vortex core (VSL and VSR in Fig. 2, which hereafter are referred to as left and right vortex shocks, respectively, following Hillier[7]). In Fig. 2, which presents the initial stage of flow development, the rollup of the shear layer due to the Kelvin–Helmholtz instability is not yet observed.

Figures 3a–3d show subsequent development of the flowfield near the corner. A bifurcated structure of the vortex shocks, especially of the left vortex shock is prominent. We can see from the figures that with increasing time, the shear layer rolls up to form discrete vortices successively (Kelvin–Helmholtz instability). The sense of rotation of these vortices is clockwise. In Fig. 3 an open arrow indicates the motion of a rolled-up vortex which passes through the left vortex shock from below. After the vortex passed through the left vortex shock, one can clearly observe the generation of a new shock wave, indicated by a solid arrow in Fig. 3b, which propagates left, as seen in Figs. 3c and 3d. This phenomenon occurs every-time a rolled-up vortex passes through the vortex shock, leading the branch-like structure of the vortex shock. Similar generation of new shock waves are observed on the right vortex shock, although the phenomenon looks more complex because of the interaction of the vortex shock with the multiple shear layers which are formed in the vortical flowfield due to the swirl of the original shear layer emanated from the corner. Thus, we may say that the generation and propagation of the shock waves, due to the successive interaction of rolled-up vortices with the vortex shocks, is a mechanism responsible for a formation of a branch-like structure of the secondary shock wave.

The appearance of the vortex shocks are dependent on M_S. As an example, flowfields near the corner for the cases of $M_S = 1.3$ and 1.7 are presented in Fig. 4. When the incident shock wave is weak, as seen in Fig. 4a, vortex shocks are not formed, although the shear layer suffers from the Kelvin–Helmholtz instability and rolls up to form discrete vortices. On the other hand, with a strong incident shock wave, as seen in Fig. 4b, the shock wave along the shear layer (SW1), the rolled-up vortices, and the vortex shocks are also strong and the interactions among these lead to a more complex flowfield. However, the mechanism of the branch-like structure of

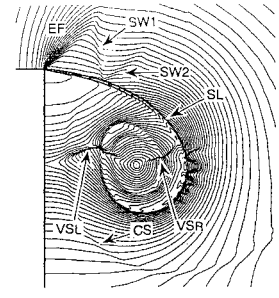

Fig. 2 Flowfield near the corner, density contours, $M_S = 1.5, \bar{t} = 0.64$.

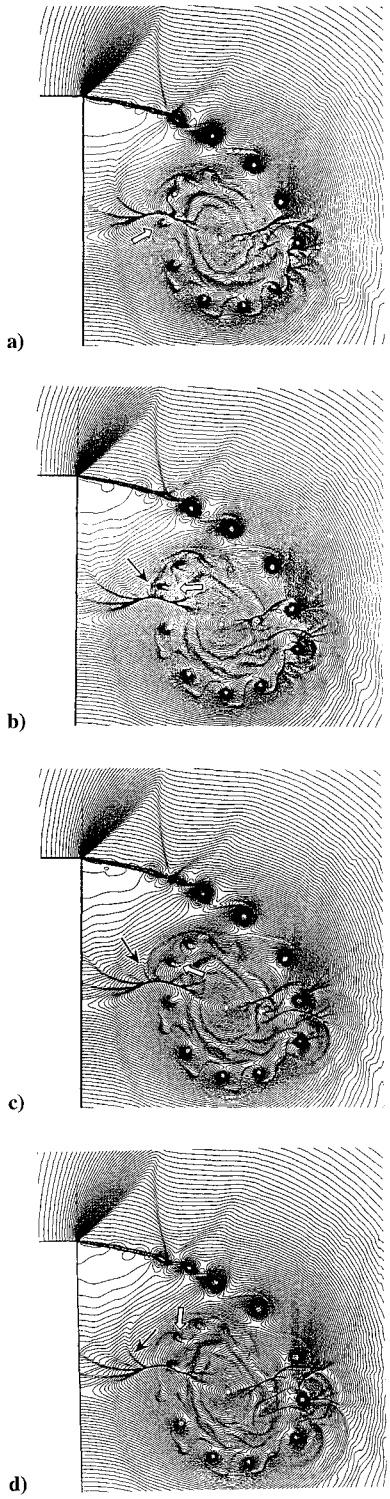

Fig. 3 Density contours near the corner, M_S = 1.5: a) $\bar{t}$ = 0.956, just before vortex hits the left vortex shock, b) $\bar{t}$ = 0.987, just after the vortex passed through the left vortex shock, c) $\bar{t}$ = 1.001, and d) $\bar{t}$ = 1.026.

the vortex shocks is essentially unchanged from the weaker case of $M_S = 1.5$.

The numerical study of Meadows et al.[8] in a planar shock wave interaction with a single vortex indicates that the interaction with a strong enough vortex causes not only the deformation but also the branching of the shock wave. The pattern of shock wave branching obtained by Meadows et al. is similar to that of the present result, especially on the left vortex shock. Also, high-resolution shadowgraphs of Schmidt and Duffy in Fig. 12 as presented in Ref. 9 clearly show the similar shock wave bifurcation inside the vortex ring formed by shock wave emission from an open-ended shock tube.

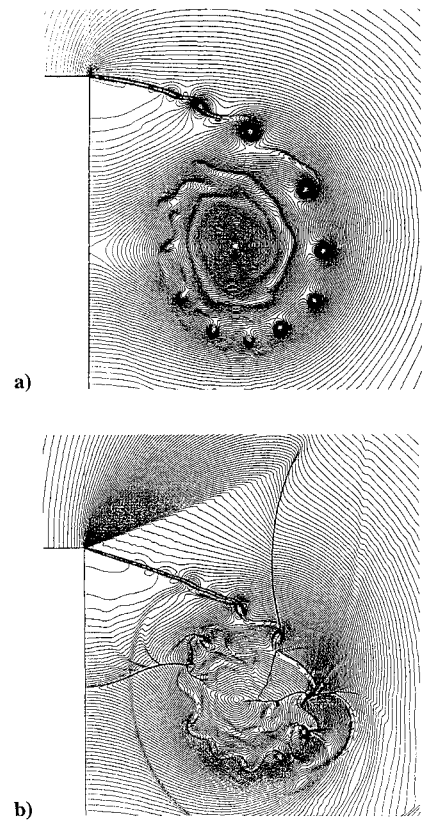

Fig. 4 Density contours near the corner: a) M_S = 1.3, $\bar{t}$ = 1.312, and b) M_S = 1.7, $\bar{t}$ = 0.800.

Conclusions

Shock wave diffraction over a 90-deg sharp corner was numerically studied with special interest in the evolution of the corner vortex. By applying the AMR algorithm to this problem, the fine structures of the vortical flowfield are captured for the first time. The computational results show the growth of the Kelvin–Helmholtz instability along the shear layer. A successive interaction between the rolled-up vortices caused by the instability and the vortex shocks is found to be responsible for the bifurcated structure of the vortex shocks.

Acknowledgments

The first author was supported by a JSPS Fellowship for Japanese junior scientists. The computations were performed on Cray Y-MP8 of Institute of Fluid Science (IFS), Tohoku University. The authors would like to acknowledge the help of Takeshi Satoh of Nissan Motor Co., Ltd., and Yuji Hattori of IFS, Tohoku University, in performing the computations.

References

[1]Uchiyama, N., and Inoue, O., "Adaptive Mesh Refinement Computation of Compressible Flow," *Proceedings of the 19th International Symposium on Shock Waves* (to be published).

[2]Berger, M. J., and Colella, P., "Local Adaptive Mesh Refinement for Shock Hydrodynamics," *Journal of Computational Physics*, Vol. 82, 1989, pp. 64–84.

[3]Takayama, K., and Inoue, O., "Shock Wave Diffraction over a 90 Degree Sharp Corner," *Shock Waves*, Vol. 1, 1991, pp. 301–312.

[4]Uchiyama, N., and Inoue, O., "On the Performance of Adaptive Mesh Refinement Computation," *Shock Waves*, Vol. 2, 1992, pp. 117–120.

[5]Steger, J. L., and Warming, R. F., "Flux Vector Splittings of the Inviscid Gasdynamic Equations with Application to Finite-Difference Methods," *Journal of Computational Physics*, Vol. 40, 1981, pp. 263–293.

[6]Van Leer, B., "Towards the Ultimate Conservative Difference Scheme. IV. A New Approach to Numerical Convection," *Journal of Computational Physics*, Vol. 23, 1977, pp. 276–299.

[7]Hillier, R., "Computation of Shock Wave Diffraction at a Ninety Degree Convex Edge," *Shock Waves*, Vol. 1, 1991, pp. 89–98.

[8]Meadows, K., Kumar, A., and Hussaini, M. Y., "A Computational Study on the Interaction Between a Vortex and a Shock Wave," *AIAA Journal*, Vol. 29, No. 2, 1990, pp. 174–179.
[9]Wang, J. C. T., and Windhopf, G. F., "Numerical Simulation of Blast Flowfields Using a High Resolution TVD Finite Volume Scheme," *Computers and Fluids*, Vol. 18, No. 1, 1990, pp. 103–137.

Active Control of Vortex Breakdown over a Delta Wing

I. Gursul,* S. Srinivas,† and G. Batta*
University of Cincinnati, Cincinnati, Ohio 45221-0072

Introduction

THE objective of this study is to accomplish active control of vortex breakdown over delta wings. The first step in this effort is to identify a physical quantity that indicates the existence of vortex breakdown and can be used as a feedback signal for active control. Previous studies[1,2] suggest that pressure fluctuations induced by the helical mode instability of vortex breakdown is a good candidate. Measurement of pressure fluctuations at a single location on the wing surface can be sufficient for control purposes. The variation of the amplitude of pressure fluctuations (or rms value of pressure) with the breakdown location seems monotonic.[2] Hence, in this study, the rms value of pressure was chosen as the control variable, and a feedback control strategy was considered.

The second element in active control of vortex breakdown is to identify a flow controller to influence the vortex breakdown location. Several methods were shown to delay vortex breakdown. Blowing and suction in the tangential direction along the leading edge,[3,4] suction applied around the vortex axis,[5,6] and use of leading-edge flaps[7] are among them. For most of the techniques mentioned, however, the relationship between the control parameter and the vortex breakdown location is unknown or undesirable (i.e., not monotonic). A desirable controller should have a monotonic relationship between the control parameter and breakdown location. Sweep angle has such a relationship. Therefore, variable sweep angle control was employed in this study. The relationship between the sweep angle and vortex breakdown location is very well known from static experiments.

A delta wing with variable sweep was fabricated (see Fig. 1a). Measured rms value of pressure coefficient at a fixed point close to the trailing edge ($x/c = 0.94$, $y/c = 0.27$) is shown as a function of angle of attack and sweep angle in Fig. 1b. The flat region near $\Lambda = 70$ deg shows the pressure fluctuation level in the absence of the vortex breakdown over the wing ($C_p \cong 0.05$). With increasing angle of attack or decreasing sweep angle, the vortex breakdown moves over the wing as the rms pressure level increases and finally reaches a saturation. This approximate monotonic relation between the sweep angle Λ and rms C_p suggests that a feedback control may be feasible. The increase in pressure fluctuations with the decreasing sweep angle is due to the increasing length of the breakdown region over the wing, as well as increasing circulation of the leading-edge vortex.[8]

An important consideration for the feedback control is the system dynamic response. It is well known that the dynamic response of the vortex breakdown location in unsteady flows is characterized by time-lag effects. It was suggested that the response of the breakdown location is similar to that of a first-order system.[8] Estimated values of the time constant for different types of motion are summarized in Ref. 8. Flow-visualization experiments[7] for variable sweep angle in a water channel showed that the normalized time constant is

Received Dec. 12, 1994; revision received May 18, 1995; accepted for publication June 1, 1995.

*Assistant Professor, Department of Mechanical, Industrial and Nuclear Engineering.
†Graduate Student, Department of Mechanical, Industrial and Nuclear Engineering.

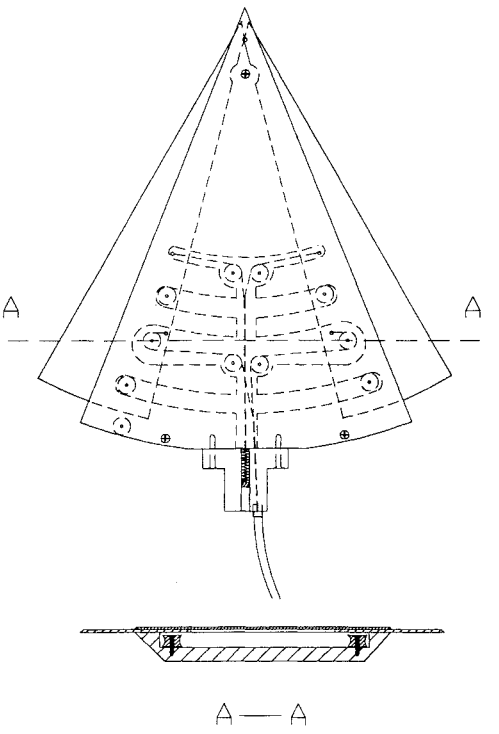

Fig. 1a Schematic of variable sweep delta wing.

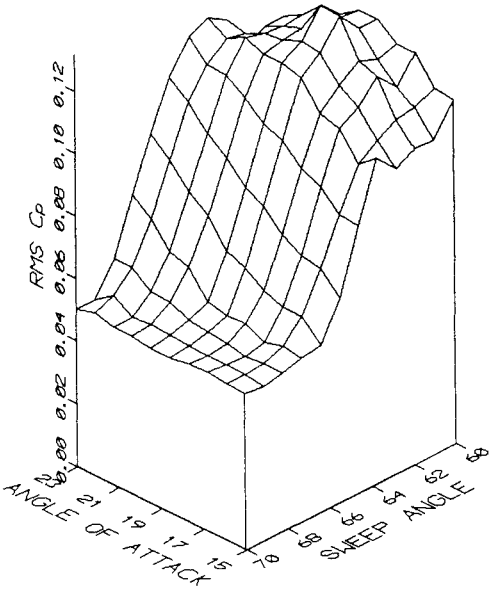

Fig. 1b RMS value of pressure coefficient as a function of angle of attack and sweep angle.

$\tau U_\infty/c = 2$–7. The idealization as a first-order system suggested that either proportional or integral control (or a combination of both) could be suitable for this application.

Experimental Setup

Experiments were carried out in a closed-circuit wind tunnel with a cross-sectional area of 61 by 61 cm. Details of the experimental setup and model can be found in Ref. 8. The chord length of the wing shown in Fig. 1a was $c = 268$ mm and the Reynolds number was $Re = 190{,}000$. The range of sweep angle was from $\Lambda = 60$ to $\Lambda = 70$ deg. Two thin plates were used to change the sweep angle. The motion of the plates was guided with a cable-pulley-pin system. A bicycle brake cable, whose sheath was fixed near the trailing edge and outside the wind tunnel, was attached to a drum, which was driven by a dc motor servo system. This flexible system allowed the use of variable sweep even for a pitching motion of the delta wing. The unsteady surface pressure was measured by a high-sensitivity